Microstructural Stability in Irradiated Materials

Phase Field Model Development for Microstructure and Compositional Changes under Irradiation

Anter EL-AZAB
Florida State University

Collaborations:
S. Rokkam, S. Dubey, J. Deng, T. Hochrainer
D. Wolf (ANL) & P. Millett (INL)

Acknowledgments

– BES Computational Materials Science Network (expired)

– INL LDRD via D. Wolf (summer support, 2008-2009)

– DOE-NE Fuel Cycle R&D (subcontract from INL)

– BES EFRC on Materials Science of Nuclear Fuel

Mesoscale is where material complexity shows

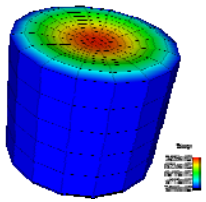

Engineering models

BC for RVE models

Mesoscale models

$\mathscr{L}u = f$ in Ω

$u = g$ on Γ

$u = \bar{u} + u'$

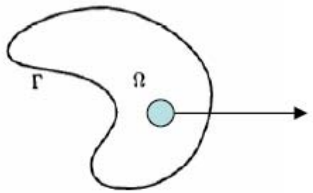

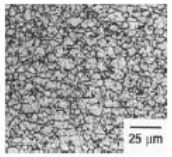

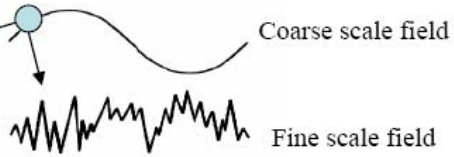

Data for effective response models

Fundamental data & statistical mechanics models

Mesoscale models fold the fundamental materials properties with the microstructure complexity to predict and understand the macroscopic response of materials …

continuum in irradiated materials

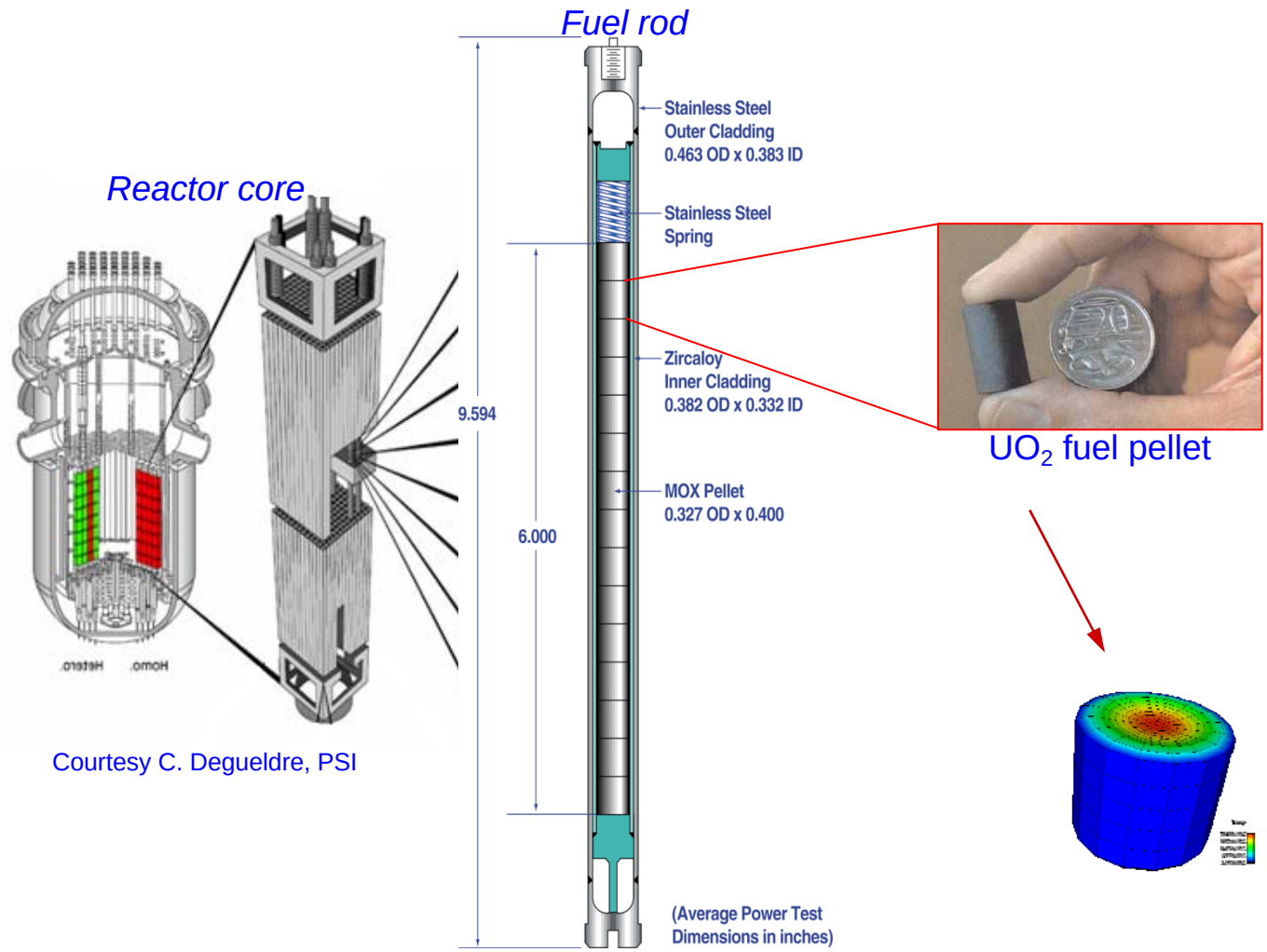

Courtesy C. Degueldre, PSI

Courtesy J. Carmack, INL

mesoscale in irradiated materials

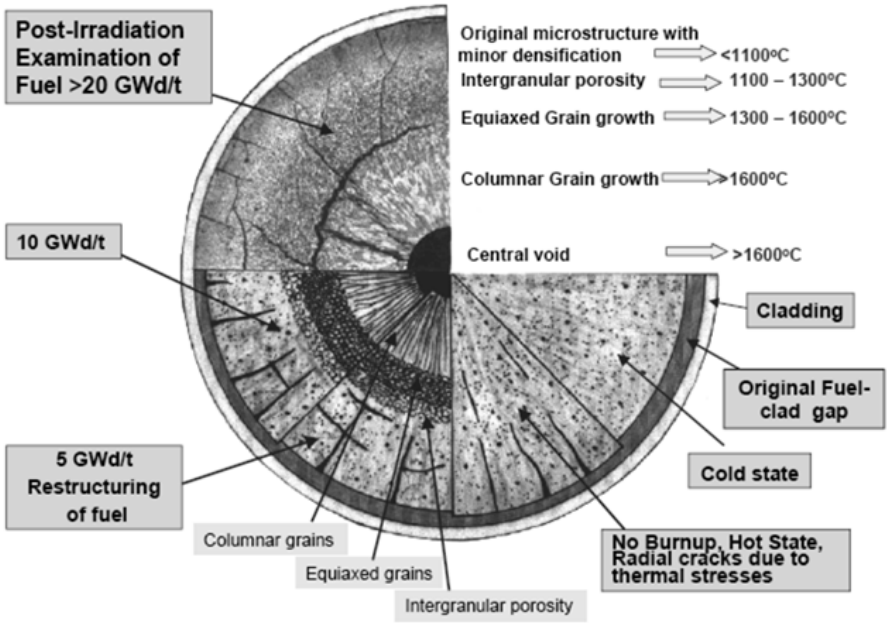

Fuel pellet

Structural materials

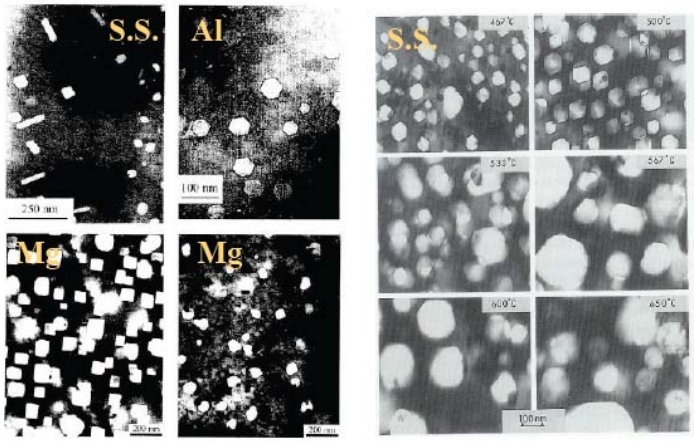

Statement of mesoscale modeling problem

Given the radiation damage parameters, stress and temperature conditions, chemical environment, model the dynamics of:

- Structural defects
- Compositional change and phase changes
- Behavior of gaseous species
- Interfacial dynamics (GB motion, clad/fuel interactions, etc)
- Elastic state and deformation history

The phase field framework

- Resolves the space and time dynamics of radiation damage, diffusion, and microstructure and micro-chemical changes in irradiated materials

- Easy to represent point defect and atomic species and incorporate microstructure features

- Captures the synergy among all defect and microstructure processes

- Stress, electrostatic, and temperature effects easily incorporated

- Framework already developed for some model systems; the level of complexity being increased to tackle complex situations

- Input can be connected with the lower scale material data/models; output corresponds (one-to-one) to with experimental observables

typical phase field model

From a free energy functional, we derive kinetic equations for composition and microstructure following Onsager formalism of non-equilibrium T.D.

$$F[c,\eta] = \int_{\Omega} f(c,\eta)\, d\Omega$$

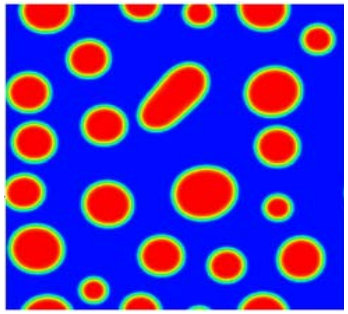

$$\frac{\partial c}{\partial t} = \nabla \cdot M \nabla \frac{\delta F}{\delta c} + \xi(\mathbf{x},t)$$

Cahn-Hilliard Eq.

$$\frac{\partial \eta}{\partial t} = -L \frac{\delta F}{\delta \eta} + \zeta(\mathbf{x},t)$$

Allen-Cahn (G.L.) Eq.

phase field model for irradiated materials

Appropriate sources and defect reactions are added to represent the irradiation environment and defect process:

modified Cahn-Hilliard Eq.

$$\frac{\partial c}{\partial t} = \nabla \cdot M \nabla \frac{\delta F}{\delta c} + \xi\left(\mathbf{x}, t\right) + G(\mathbf{x}, t) - R(\mathbf{x}, t)$$

modified Allen-Cahn (G.L.) Eq.

$$\frac{\partial \eta}{\partial t} = -L \frac{\delta F}{\delta \eta} + \zeta\left(\mathbf{x}, t\right) + \zeta_{Irrad}\left(\mathbf{x}, t\right)$$

Status of phase field modeling

pure metal

models and initial results obtained

Vacancies

Vacancies + Interstitials

Vacancies + Interstitials + Gas atoms

Grain boundaries

Swelling and Gas Behavior

models under development

Stress effects

Dislocations

Swelling, Gas Behavior, Creep

binary alloy

models and initial results obtained

Vacancies + Interstitials
Species Redistribution

Phase Change

models under development

Gas atoms
Stress effects
Dislocations
Grain boundaries

Swelling, Microchemistry, Gas Behavior, Creep

oxide fuel

model complete

Vacancies + interstitials (sub-lattices)
Electrostatics
Microstructure
Fission products

models under development

Stress effects
Dislocations
Grain boundaries

Microstructure, Compositional Changes, Gas Behavior

Challenges

- Free energy models are difficult to develop

- Fixing model parameters require non-simple mathematical analysis of the model to guarantee equivalence with sharp-interface physics models

- Handling the complexity of the complete problem: coupled radiation damage, diffusion, microstructure and composition changes, with stress and electrostatic effects

Illustration for void nucleation and growth

- **Sharp interface model for void growth**
- **Phase field model for void nucleation and growth**
- **Asymptotic analysis and model parameter determination**
- **Thermodynamic underpinning**
- **Gas bubble nucleation and growth**
- **Results**

Classical sharp interface model

- Voids grow (shrink) depending on flux of point defects. The growth model consists of 3 equations:

- Growth rate of void size:

$$\dot{R} = \frac{dR}{dt} = \frac{\Omega}{R}\left\{D_v\left[C_v - C_v^{eq}\exp\left(\frac{2\gamma\Omega}{RkT}\right)\right] - D_iC_i\right\}$$

- Rate equations for point defect (mean) fields derived using theory of sink strength:

$$\nu\Sigma_s\phi = 4\pi RND_v\left[C_v - C_v^{eq}\exp\left(\frac{2\gamma\Omega}{RkT}\right)\right] + Z_v\rho_N D_v\,(C_v - C_v^{eq}) + Z_v\rho_l D_v\left[C_v - C_v^{eq}\exp\left(-\frac{K}{2(m_i)^{1/2}\,kT}\right)\right] + 4\pi R_pN_pD_vC_v + k_{iv}C_iC_v$$

$$\nu\Sigma_s\phi = 4\pi RND_iC_i + Z_i\,(\rho_N + \rho_l)\,D_iC_i + 4\pi R_pN_pD_vC_v + k_{iv}C_iC_v$$

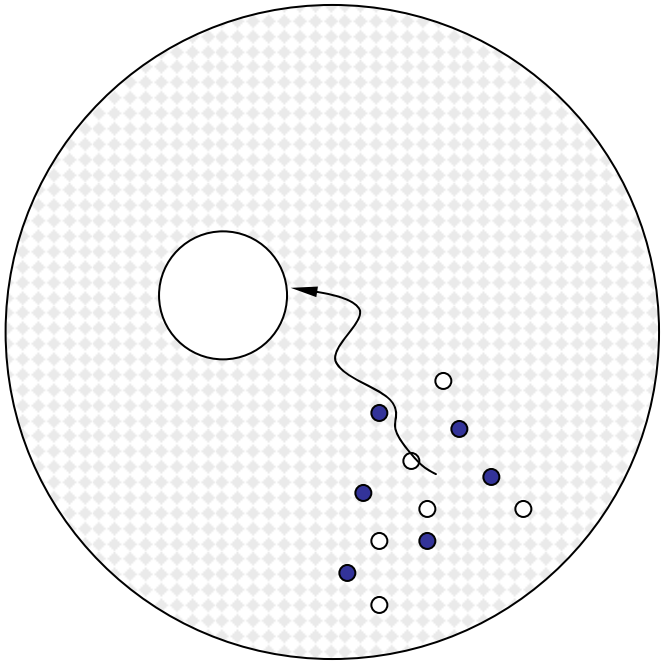

Diffuse interface (phase field) model

– Interface between void and matrix is diffuse (but has small width)

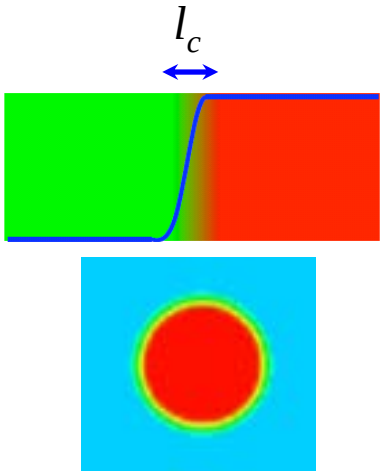

– Setting sources and sinks aside, the Chan-Hilliard and Allen-Cahn equations are

$$\frac{\partial c_v}{\partial t} = \nabla \cdot M_v \nabla \mu_v, \quad \frac{\partial c_i}{\partial t} = \nabla \cdot M_i \nabla \mu_i, \quad \frac{\partial \eta}{\partial t} = -L\mu_\eta$$

with $$\mu_v = \frac{1}{N}\frac{\delta F}{\delta c_v}, \quad \mu_i = \frac{1}{N}\frac{\delta F}{\delta c_i}, \quad \mu_\eta = \frac{\delta F}{\delta \eta}$$

$\boxed{\eta = 1 \text{ in void}}$

– Free energy functional:

$$F = N \int_\Omega \left[h(\eta)\Psi_0(c_v, c_i) + \eta^2 w(c_v, c_i) + \kappa_v |\nabla c_v|^2 + \kappa_i |\nabla c_i|^2 + \kappa |\nabla \eta|^2 \right] d\Omega$$

with

$$h(\eta) = (\eta - 1)^2, \quad w(c_v, c_i) = A(c_v - 1)^2 + Bc_i^2$$

$$\Psi_0(c_v, c_i) = E_v^f c_v + E_i^f c_i + k_B T \left[c_v \ln c_v + c_i \ln c_i + (1 - c_v - c_i) \ln (1 - c_v - c_i) \right]$$

- Ned to perform asymptotic expansion to fix model parameters.

Model input

- Formation energy of defects
- Diffusivities
- Kinetic barriers
- Thickness parameter delta
- Gradient coefficient (alpha)
- Surface energy

Quantity	Value	Value (rescaled units)
E_v^f	1.0 eV	
E_i^f	2.2 eV	
D_v°	2.5×10^{-5} m$^2/sec$	2.5×10^4 nm$^2/nsec$
D_i°	2.0×10^{-7} m$^2/sec$	2.0×10^2 nm$^2/nsec$
E_v^m	0.7 eV	
E_i^m	0.12 eV	
γ	1.7 J/m^2	10.6 eV$/nm^2$
Ω	$1.2 \times 10^{-29} m^3$	$1.2 \times 10^{-2} nm^3$
δ	1 nm	
ν_o	7.23×10^{13} 1/sec	7.23×10^4 1/nsec

- All well defined physical quantities.

Energy landscape (vacancies only)

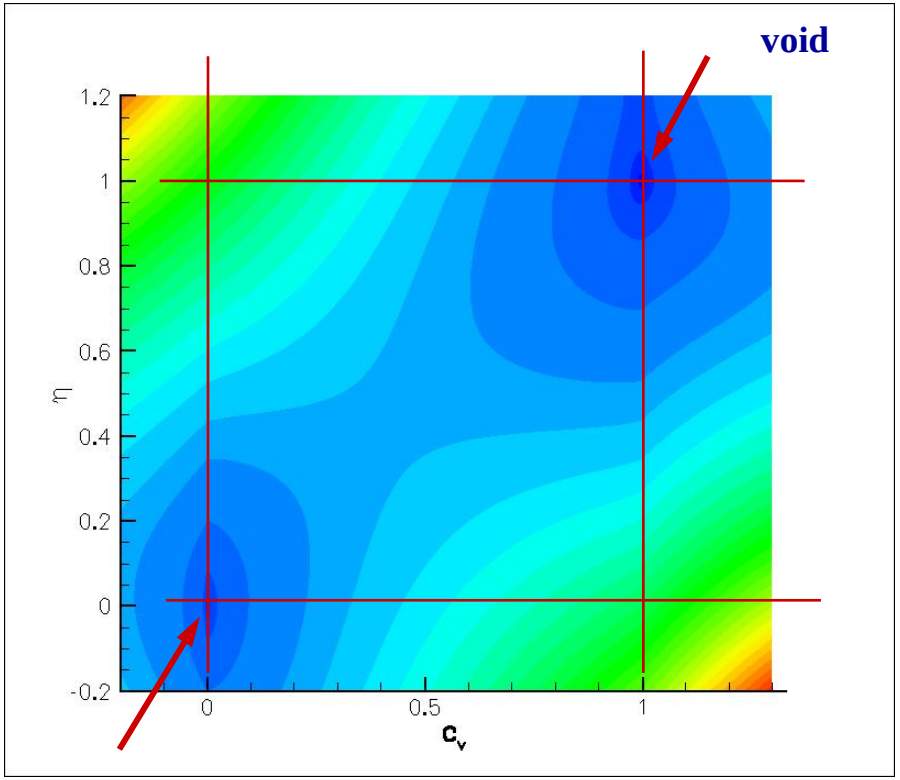

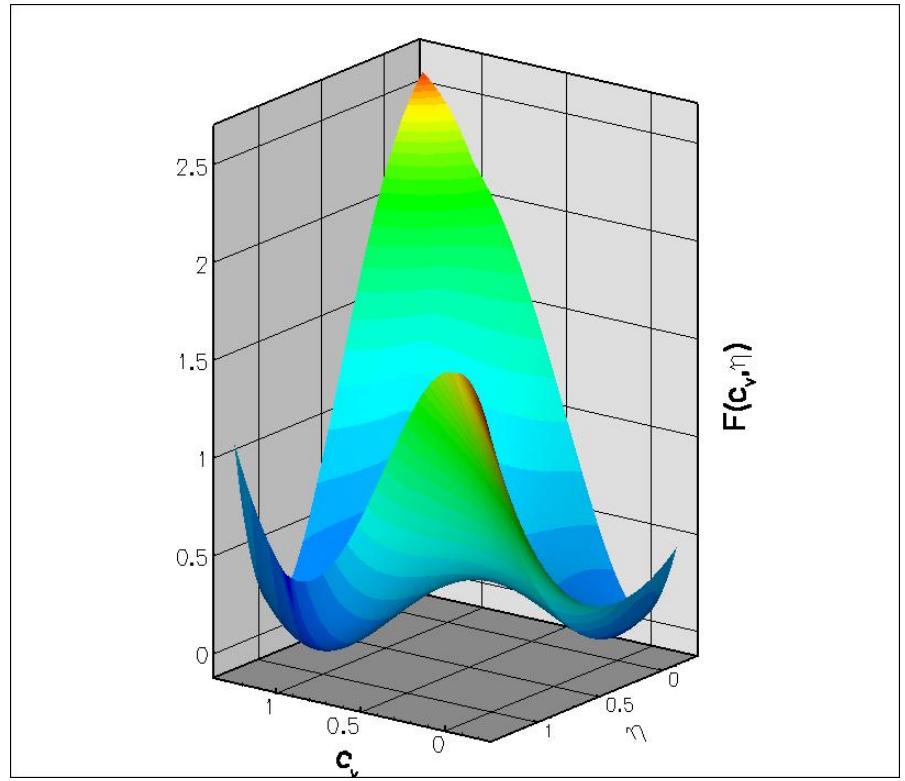

matrix with thermal equilibrium concentration

void growth and shrinkage

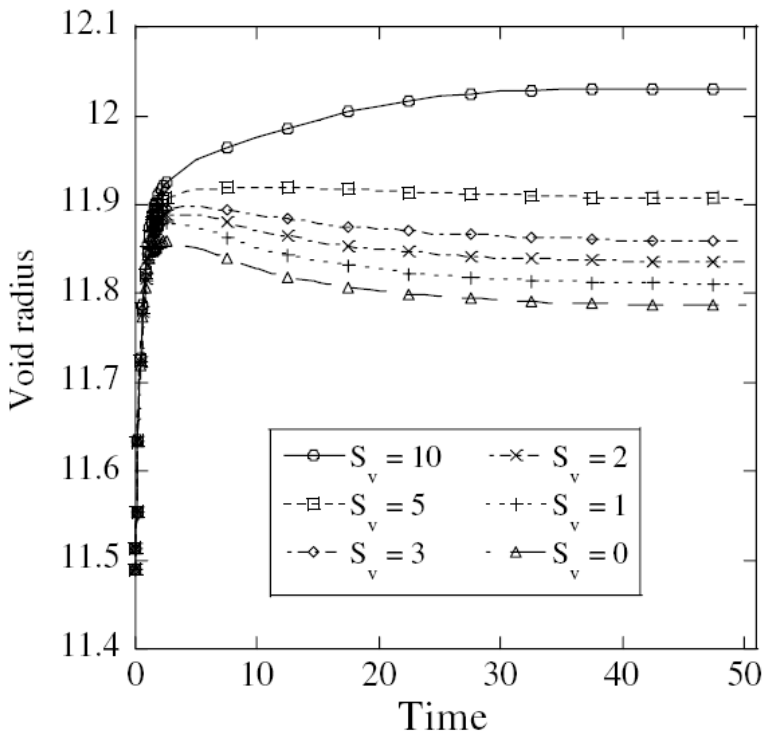

Figure 5. Void radius as a function of time for different initial vacancy supersaturation levels.

Growth and shrinkage take place depending the background concentration and the void radius

Gibbs-Thompson Effect

void growth and shrinkage

Rokkam et al.

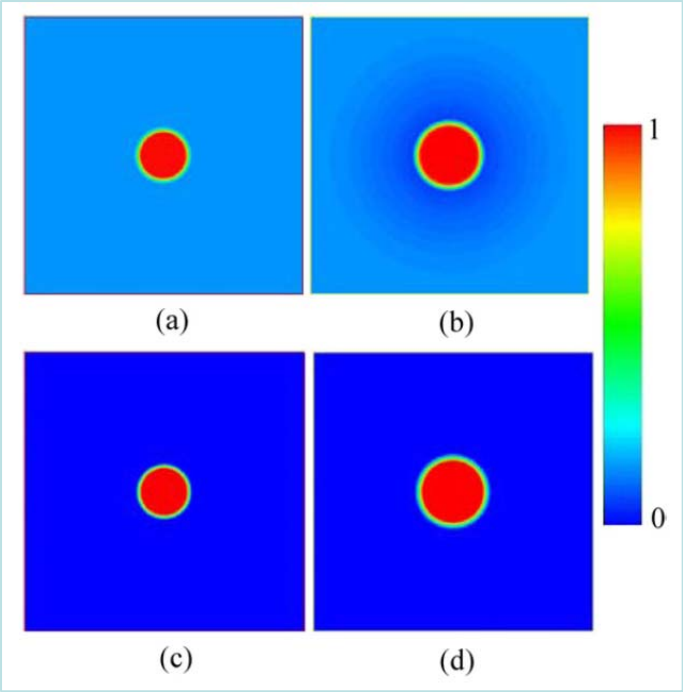

growth

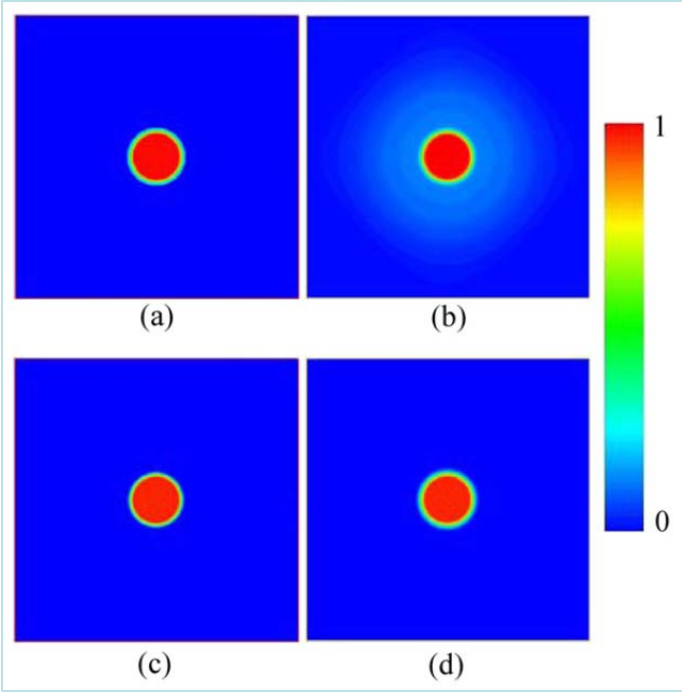

shrinkage

void-void interaction

Rokkam et al.

Ostwald ripening example

Large voids grow at the expense of small ones

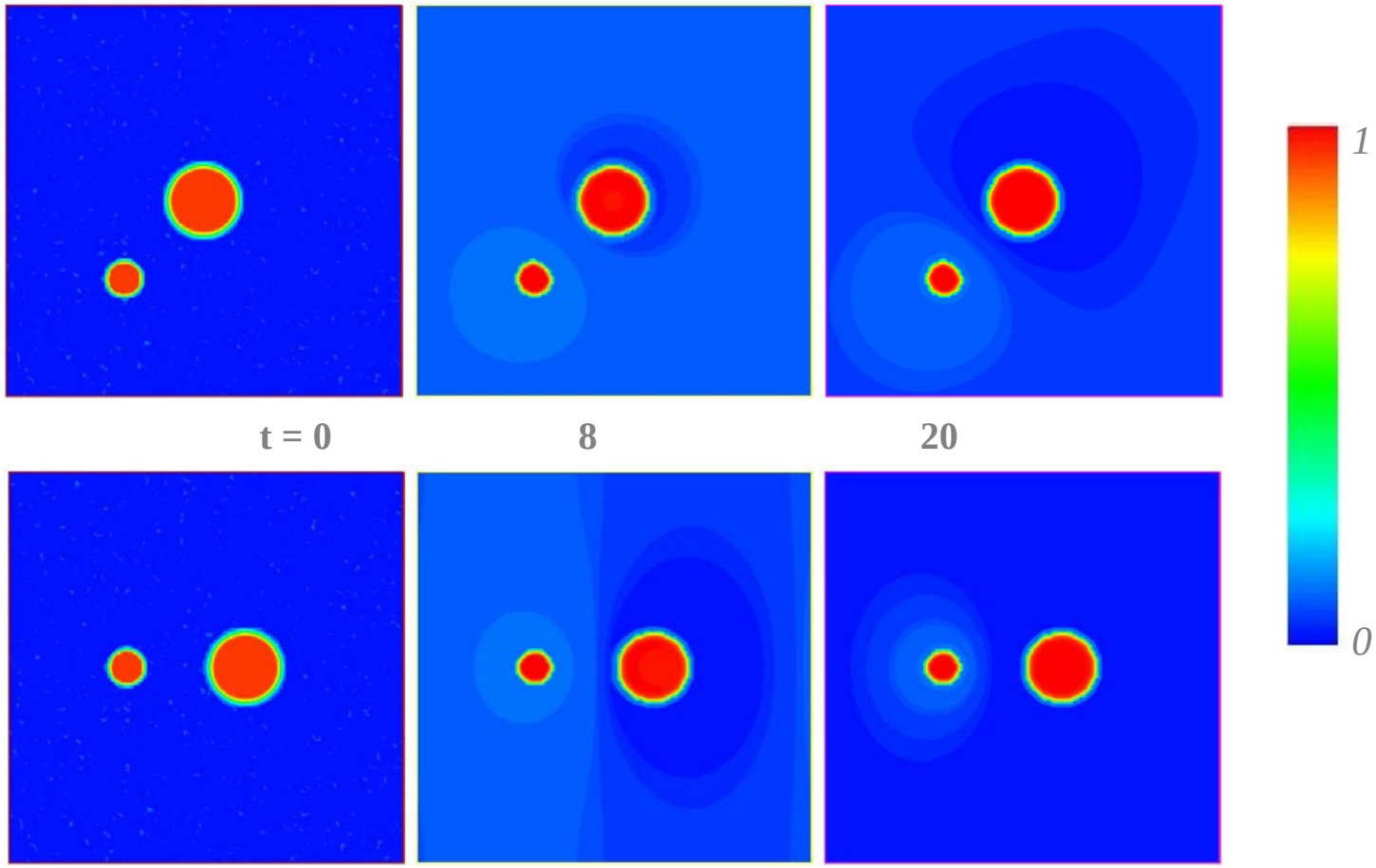

nucleation of voids under vacancy generation

Rokkam et al.

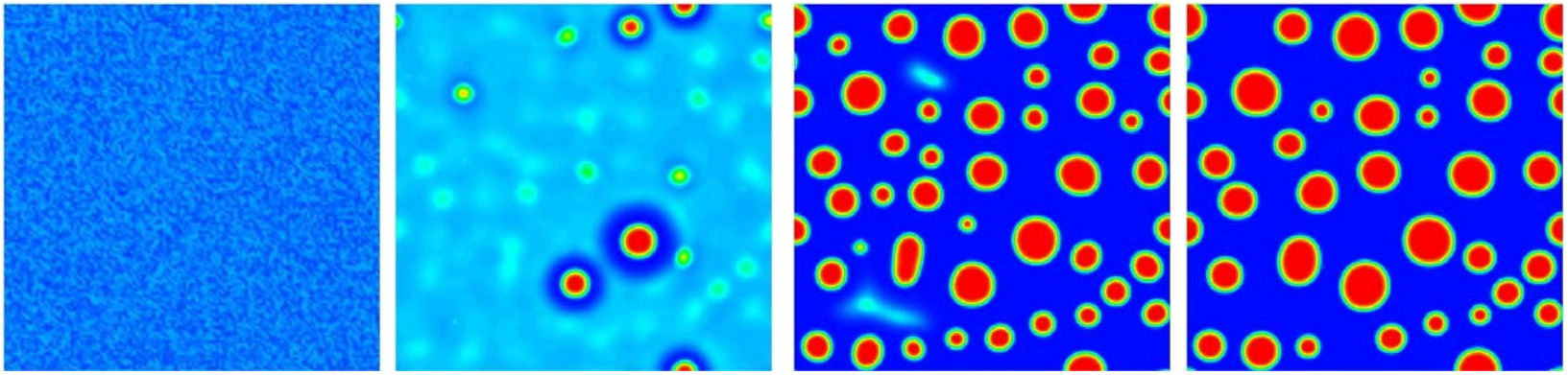

t = 0 165 190 250

Vacancy field evolution showing void nucleation due to radiation induced vacancies

Voids nucleate due to fluctuations in the vacancy concentration field. The nucleation process is homogeneous

analysis of nucleation and growth

Rokkam et al.

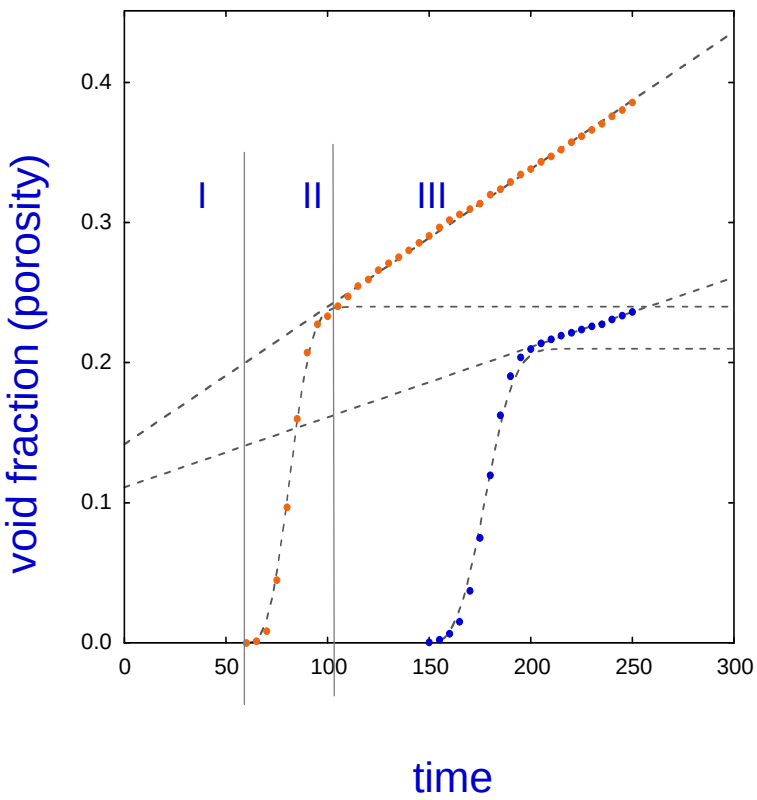

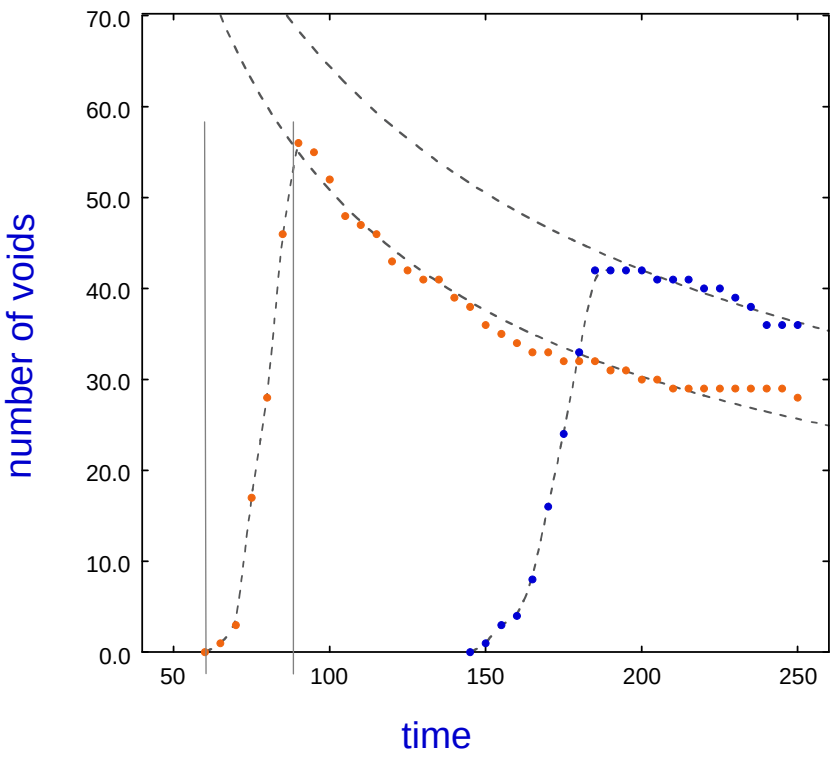

nucleation close to a preexisting void

Rokkam et al.

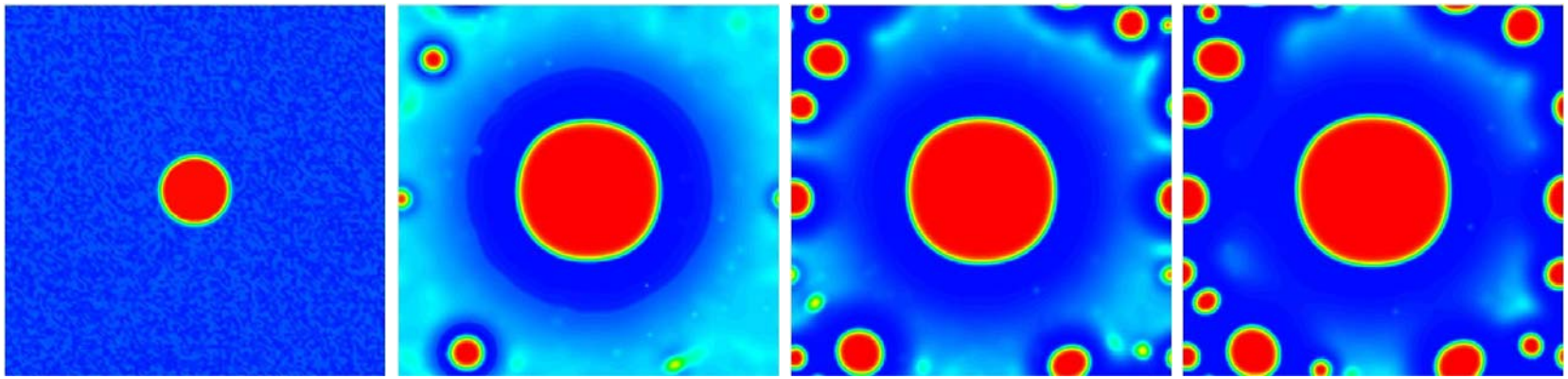

t = 0 210 240 250

Vacancy field evolution showing void growth in the presence of radiation effects

Initial void grows while new voids nucleate …

Ripening suppresses the small voids nucleating in the vicinity of the large one.

role of grain boundaries

Millett et al.

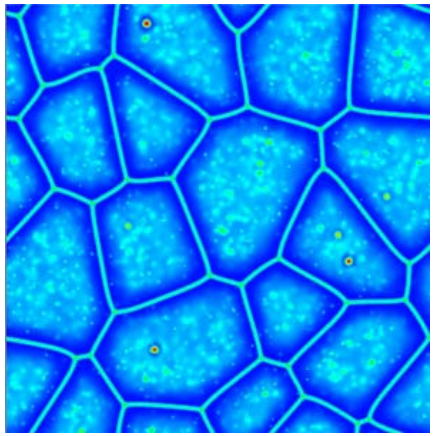

nucleation

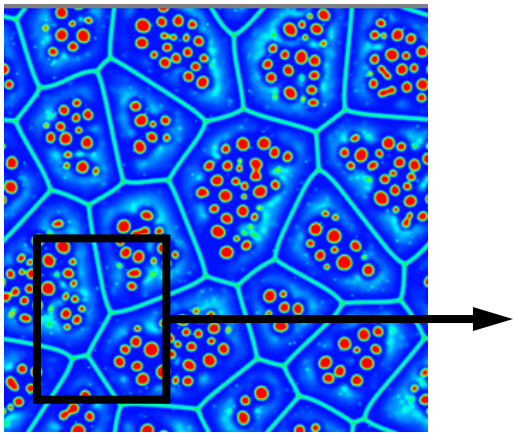

growth

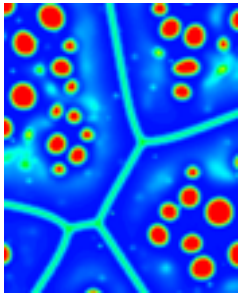

denuded GB regions

Free surfaces lead to same effect

Introducing interstitials

Rokkam et al.

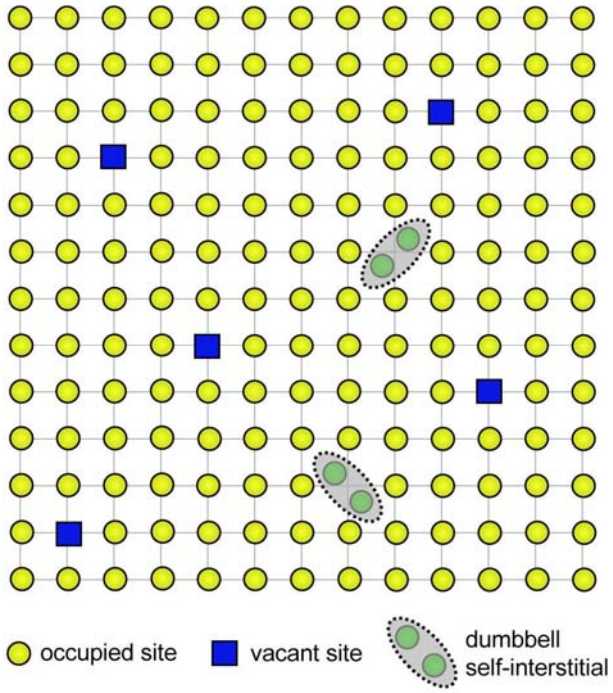

phase field model with interstitials

Energy

$$F = N\int_V \left[h(\eta) f^s(c_v,c_i) + j(\eta) f^v(c_v,c_i) + \frac{\kappa_v}{2}|\nabla c_v|^2 + \frac{\kappa_i}{2}|\nabla c_i|^2 + \frac{\kappa_\eta}{2}|\nabla \eta|^2 \right] dV$$

$$f^s(c_v,c_i) = E_v^f c_v + E_i^f c_i + k_B T[c_v \ln(c_v) + c_i \ln(c_i) + (1-c_v-c_i)\ln(1-c_v-c_i)]$$

Species

$$\frac{\partial c_v}{\partial t} = \nabla \cdot \left(M_v \nabla \frac{1}{N}\frac{\delta F}{\delta c_v} \right) + \xi(\mathbf{r},t) + P_v(\mathbf{r},t) - R_{iv}(\mathbf{r},t) - S_v^{GB}(\mathbf{r},t)$$

$$\frac{\partial c_i}{\partial t} = \nabla \cdot \left(M_i \nabla \frac{1}{N}\frac{\delta F}{\delta c_i} \right) + \zeta(\mathbf{r},t) + P_i(\mathbf{r},t) - R_{iv}(\mathbf{r},t) - S_i^{GB}(\mathbf{r},t)$$

Extended structural defects

$$\frac{\partial \eta(\mathbf{r},t)}{\partial t} = -L\frac{\delta F}{\delta \eta} + \varsigma(\mathbf{r},t) + P_{v,i}(\mathbf{r},t)$$

void nucleation under irradiation

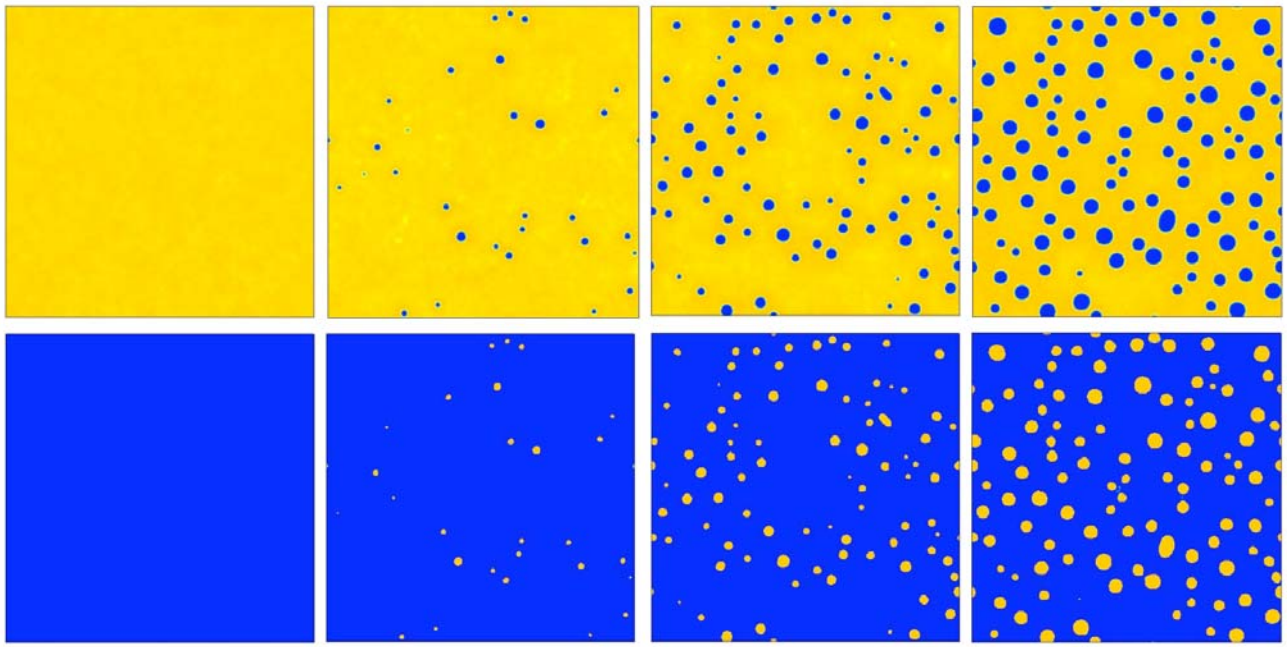

Snapshots showing the nucleation and growth of voids in the presence of dynamic cascade damage. Upper row (from left to right) illustrates the vacancy concentration field while the lower row illustrates the interstitial field. During the simulation, an interstitial production bias of 0.9 is assumed (i.e., there are 10% more vacancies introduced into the system), the net effect of which is similar to a dislocation bias. Within the voids, the vacancy concentration $c_v = 1$ and the interstitial concentration $c_i = 0$

Millett, El-Azab, Rokkam and Wolf

porosity and void density evolution

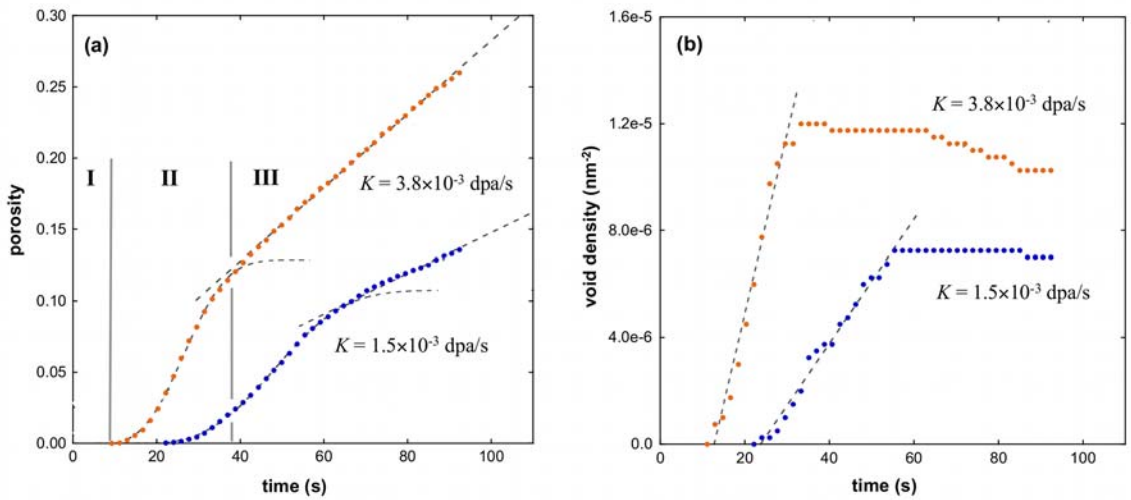

Plots of (a) the porosity and (b) the void number density throughout time for the simulation shown in Fig. 7. The orange lines represent $K = 6.4 \times 10^{-6}$ dpa/ns, while the blue lines represent $K = 2.6 \times 10^{-6}$ dpa/ns. The void evolution can be characterized by three distinct stages: I incubation, II nucleation and growth, and III coarsening. The porosity in stage II is fitted to the Johnson-Mehl-Avrami equation (Eq. (19)), and agrees quite well with the calculated values of nucleation rate, J, from (b) and the void growth rate, $\dot{R}$, from Fig. 3. In the coarsening stage, the void density saturates and decreases slightly due to Ostwald ripening.

Millett, El-Azab, Rokkam and Wolf

swelling under cascade condition

Rokkam et al.

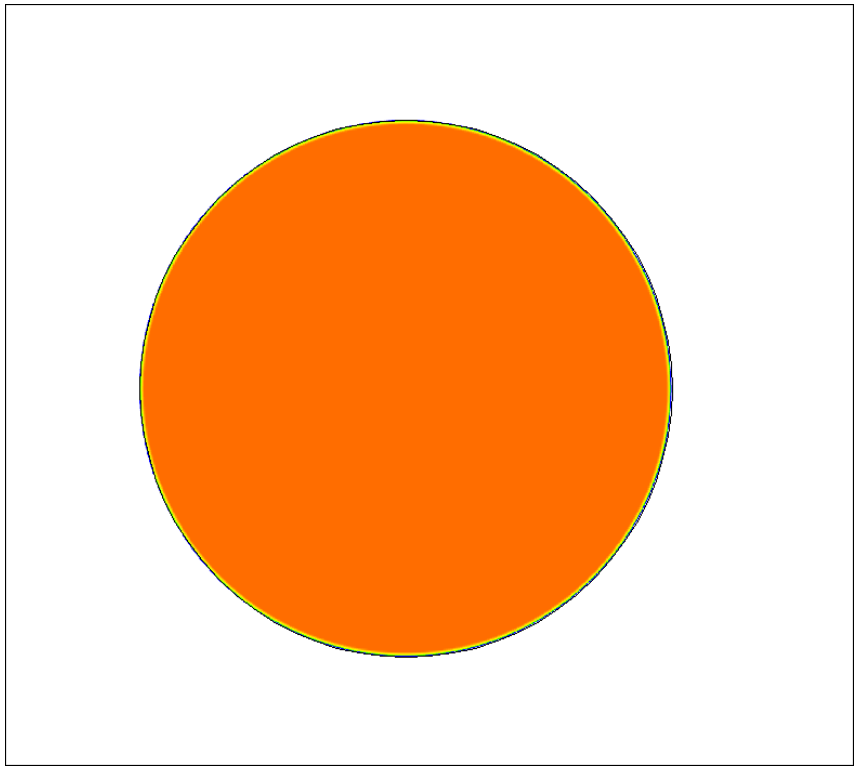

swelling under cascade condition

Rokkam et al.

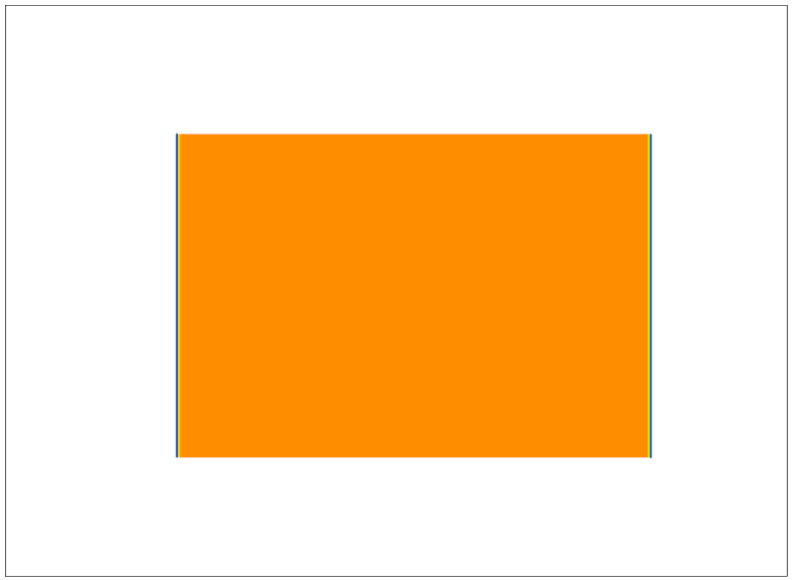

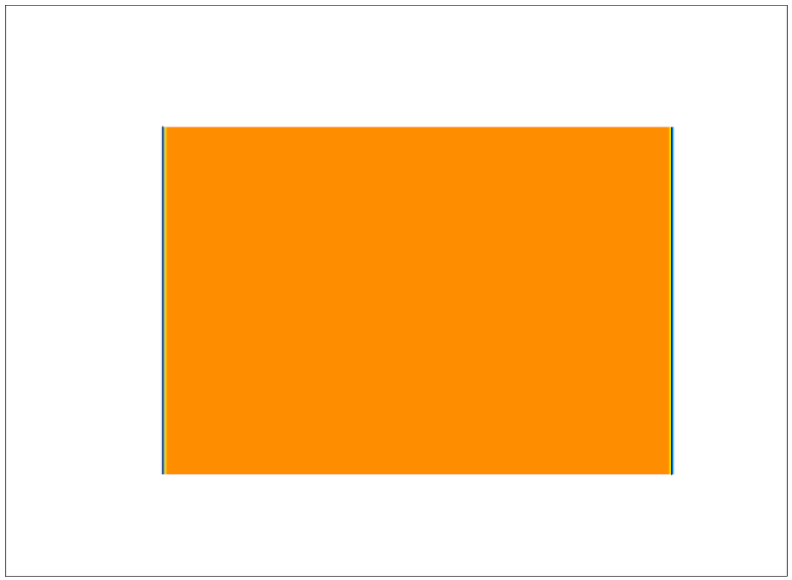

gas effects and bubble formation

Gas atoms become part of the dynamics. Governing equations become more complicated.

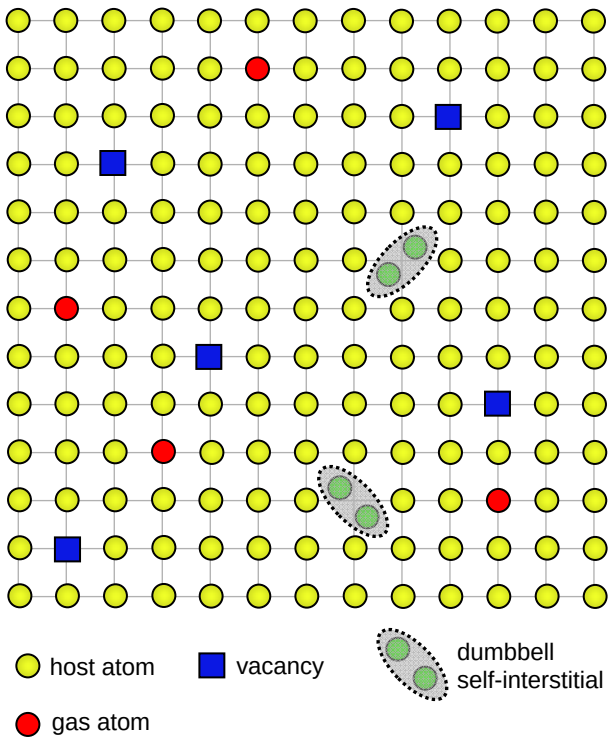

Millett, El-Azab, Wolf

Phase field model with substitutional gas atoms and GB

$$F = N\int_V \begin{bmatrix} h(\eta) f^s(c_v,c_i,c_g) + j(\eta) f^b(c_v,c_i,c_g) + \\ f^{polycr}(\eta,\phi_{1\to P}) + f^{grad}(c_v,c_i,c_g,\eta,\phi_{1\to P}) \end{bmatrix} dV$$

$$f^s(c_v,c_i,c_g) = E_v^f c_v + E_i^f c_i + E_g^f c_g + k_B T \begin{bmatrix} c_v \ln(c_v) + c_i \ln(c_i) + c_g \ln(c_g) + \\ (1-c_v-c_i-c_g)\ln(1-c_v-c_i-c_g) \end{bmatrix}$$

$$\boxed{f^b(c_v,c_i,c_g) = \left[(c_v-1)^2 + c_i^2\right] + \left[\mu_g^o c_g + c_g k_B T \ln c_g + c_g k_B T \ln(k_B T)\right]}$$

$$f^{polycrystal}(\eta,\phi_{1,\ldots,P}) = 3A\left(\sum_{k=1}^{P}\phi_k^2 + \eta^2\right)^2 - 4A\left(\sum_{k=1}^{P}\phi_k^3 + \eta^3\right)$$

$$f^{grad}(c_v,c_i,c_g,\eta,\phi_{1\to P}) = \frac{\kappa_v}{2}|\nabla c_v|^2 + \frac{\kappa_i}{2}|\nabla c_i|^2 + \frac{\kappa_g}{2}|\nabla c_g|^2 + \frac{\kappa_\eta}{2}|\nabla \eta|^2 + \frac{\kappa_\phi}{2}\sum_{k=1}^{P}|\nabla \phi_k|^2$$

$$\frac{\partial c_v}{\partial t} = \nabla\cdot\left(M_v \nabla \frac{1}{N}\frac{\delta F}{\delta c_v}\right) + \xi_v(\mathbf{r},t) + P_v(\mathbf{r},t) - R_{iv}(\mathbf{r},t) - S_v^{GB}(\mathbf{r},t)$$

$$\frac{\partial c_i}{\partial t} = \nabla\cdot\left(M_i \nabla \frac{1}{N}\frac{\delta F}{\delta c_i}\right) + \xi_i(\mathbf{r},t) + P_i(\mathbf{r},t) - R_{iv}(\mathbf{r},t) - S_i^{GB}(\mathbf{r},t)$$

$$\frac{\partial c_g}{\partial t} = \nabla\cdot\left(M_g \nabla \frac{1}{N}\frac{\delta F}{\delta c_g}\right) + \xi_g(\mathbf{r},t) + P_g(\mathbf{r},t)$$

$$\frac{\partial \eta(\mathbf{r},t)}{\partial t} = -L\frac{\delta F}{\delta \eta} + \varsigma(\mathbf{r},t) + P_{v,i}(\mathbf{r},t)$$

$$\frac{\partial \phi_i(\mathbf{r},t)}{\partial t} = -L_\phi \frac{\delta F}{\delta \phi_i}$$

Millett, El-Azab, Wolf

Millett, El-Azab, Wolf

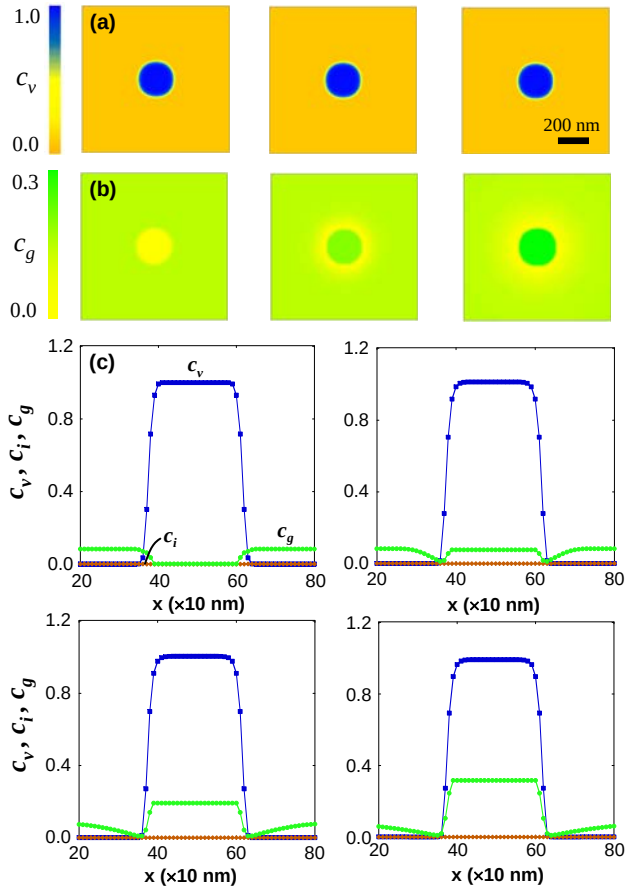

Increase of gas concentration inside an initially-empty void surrounded by a solid with a supersaturated gas concentration. The top figures show the evolution of (a) vacancy and (b) gas atom concentration fields. (c) Plots of the conserved concentration fields, c_v, c_i, c_g, along a cross-sectional slice through the centerline of the bubble throughout time. The absorption of gas atoms into the void creates a gradient in the gas concentration in the adjacent solid region.

Millett, El-Azab, Wolf

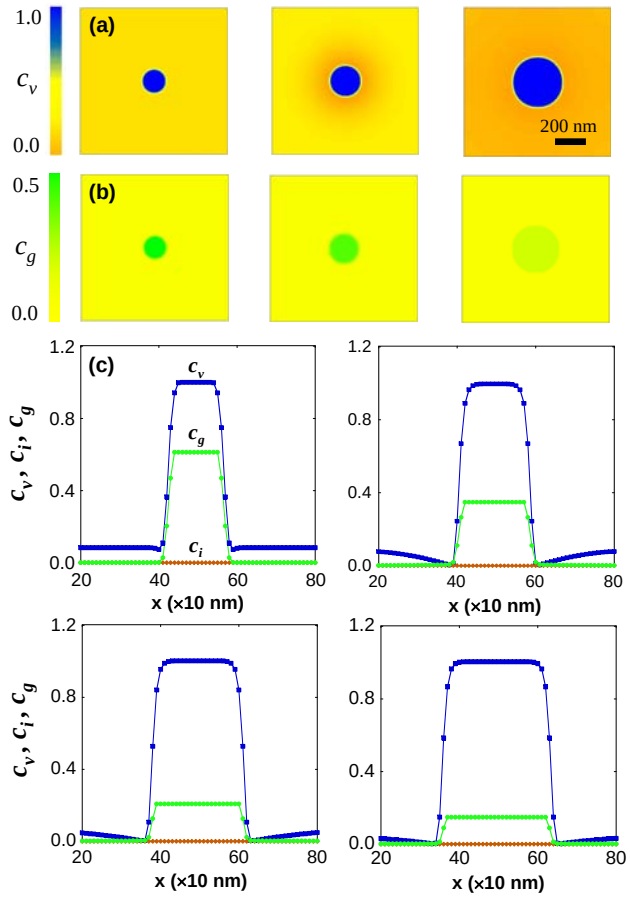

Growth of a bubble due to a supersaturated vacancy concentration in the solid. The gas concentration in the bubble, which is initially over-saturated, decreases due to the increase in bubble volume. The top figures show the evolution of (a) vacancy and (b) gas atom concentration fields. (c) Plots of the conserved concentration fields, c_v, c_i, c_g, along a cross-sectional slice through the centerline of the bubble throughout time.

Millett, El-Azab, Wolf

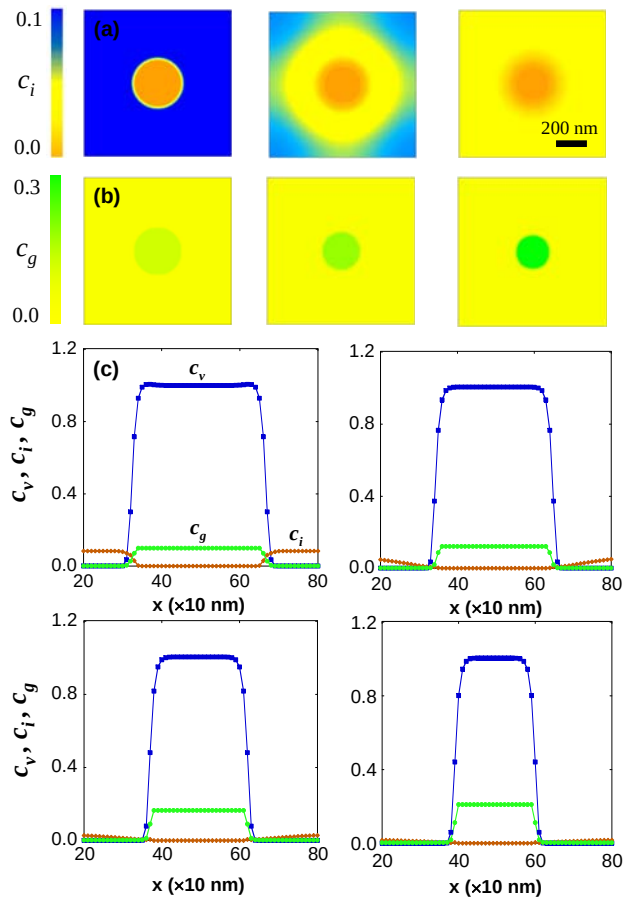

Shrinkage of a bubble due to a supersaturated self-interstitial concentration in the solid. The gas concentration in the bubble, which is initially under-saturated, increases due to the decrease in bubble volume. The top figures show the evolution of (a) vacancy and (b) gas atom concentration fields. (c) Plots of the conserved concentration fields, c_v, c_i, c_g, along a cross-sectional slice through the centerline of the bubble throughout time.

Millett, El-Azab, Wolf

Nucleation of bubbles under concurrent cascade and gas production conditions

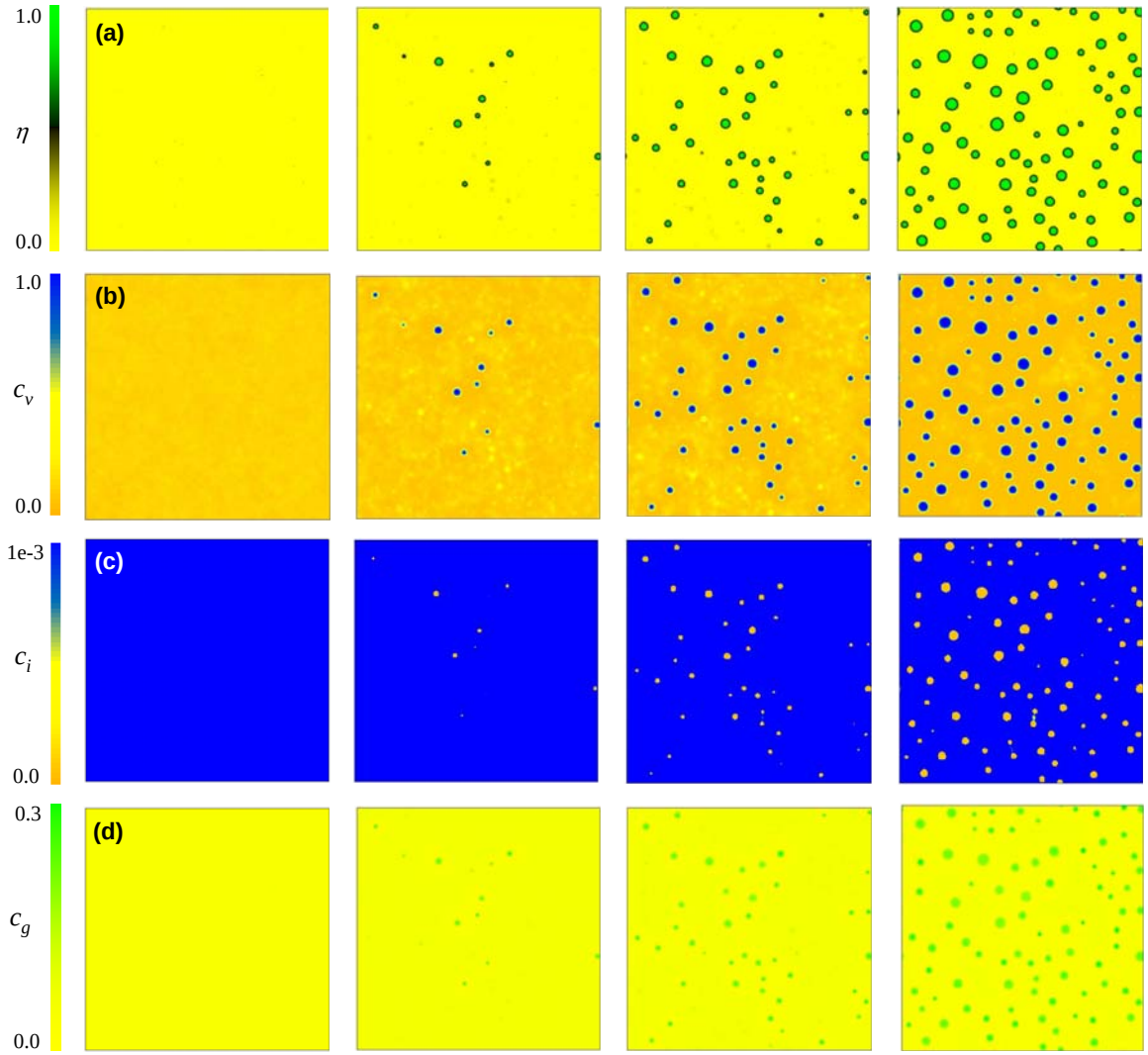

Snapshots showing the nucleation and growth of bubbles in the presence of on-going cascades modeled using Eq. (10) and gas production using Eq. (15). The top-to-bottom rows represent the (a) η, (b) c_v, (c) c_i, and (d) c_g fields. During the simulation, an interstitial production bias of 0.9 is assumed (i.e., there are 10% more vacancies introduced into the system), the net effect of which is similar to a dislocation bias. Within the voids, the vacancy concentration $c_v = 1$, the interstitial concentration $c_i = 0$, and the gas concentration varies.

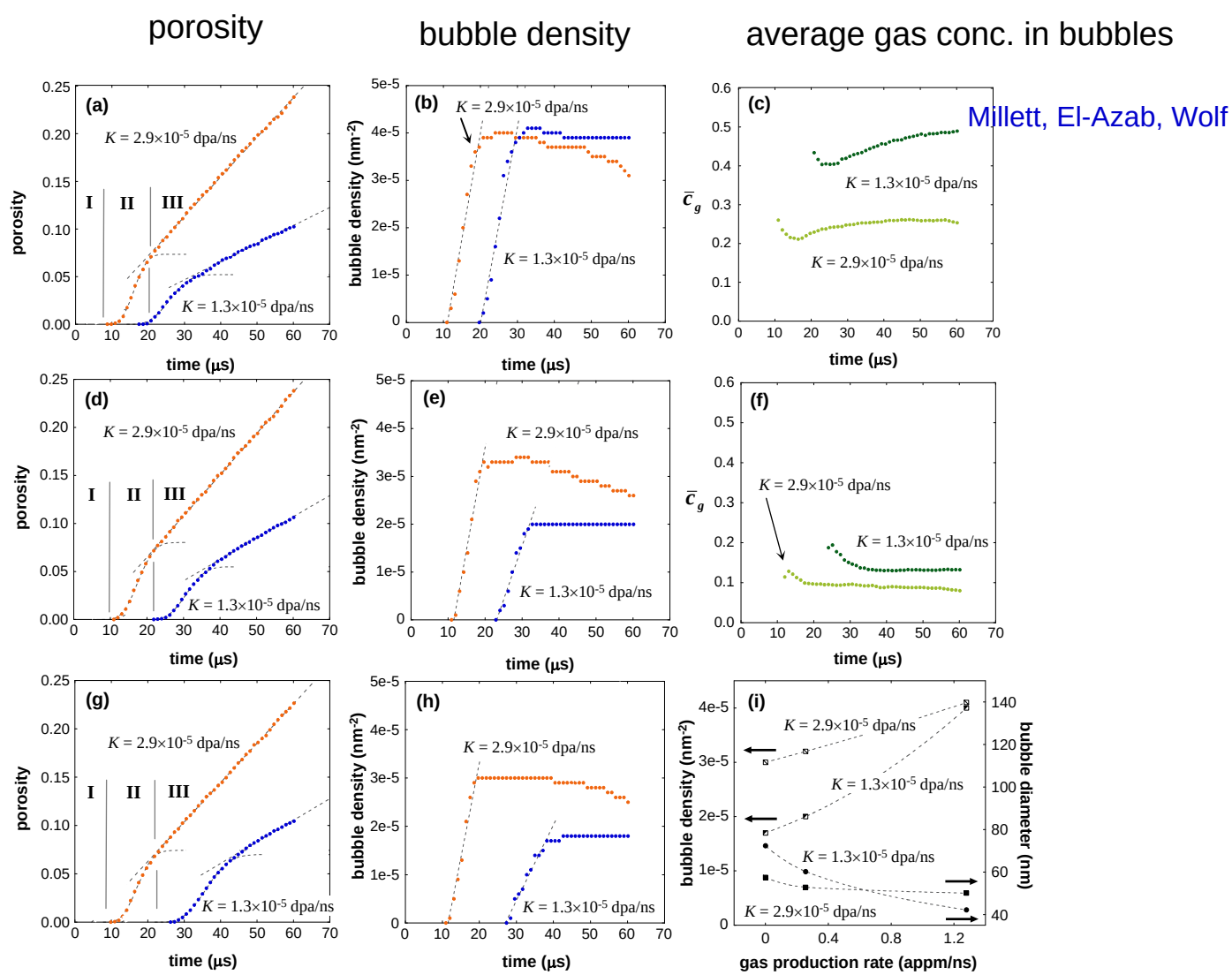

Figure 6: The evolution of (a), (d), (g) porosity, (b), (e), (h) bubble density, and (c), (f) average gas concentration inside the bubbles throughout time. The top row ((a), (b), (c)) represents a gas production rate of 1.28 appm/ns, while the middle row ((d), (e), (f)) represents a gas production rate of 0.256 appm/ns. In (g) and (h), the gas production rate is zero. As shown in (i), for increasing gas production rate, the bubble density increases while the average bubble size decreases. Also, as shown in (c) and (f), the gas concentration within bubbles decreases during stage II (nucleation and growth) due to the relatively rapid bubble growth while the bubbles are still small.

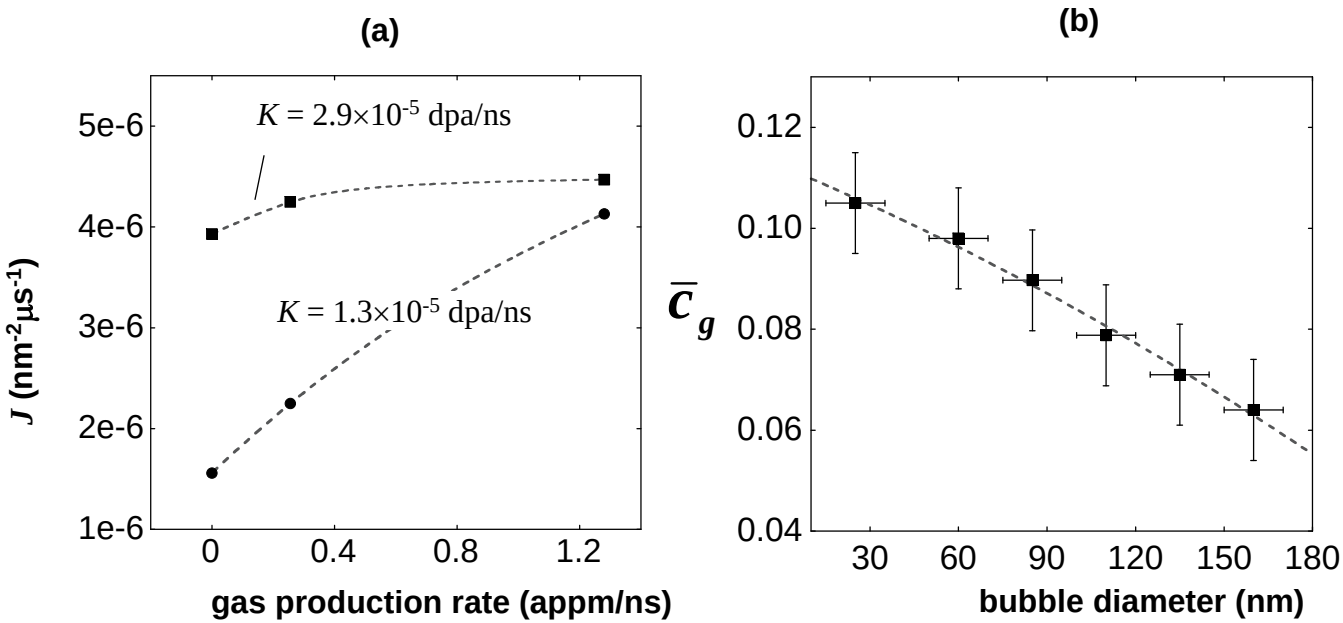

Figure 7: (a) The nucleation rate of gas bubbles increases with increasing gas production rate for both displacement rates. This effect is more dramatic for the lower displacement rate (K = 1.3 × 10^{-5} dpa/ns). (b) The average gas concentration within the bubbles decreases with increasing bubble diameter.

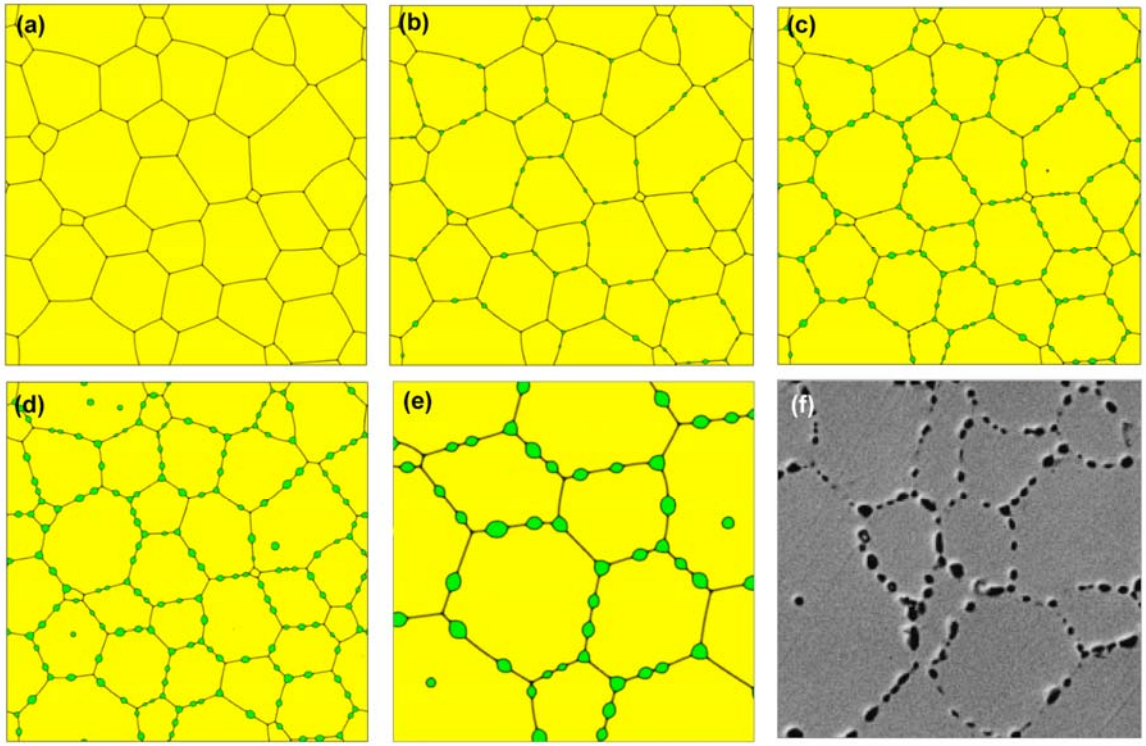

Figure 10: (a)-(d) Snapshots throughout time of the nucleation and growth of intergranular gas bubbles in a polycrystalline grain structure, while (e) is a close-up view. Bubbles existing on GBs are lenticular shaped, whereas bubbles on triple junctions have a curved triangular shape. (f) Image of intergranular bubbles in UO_2 taken from [ref].

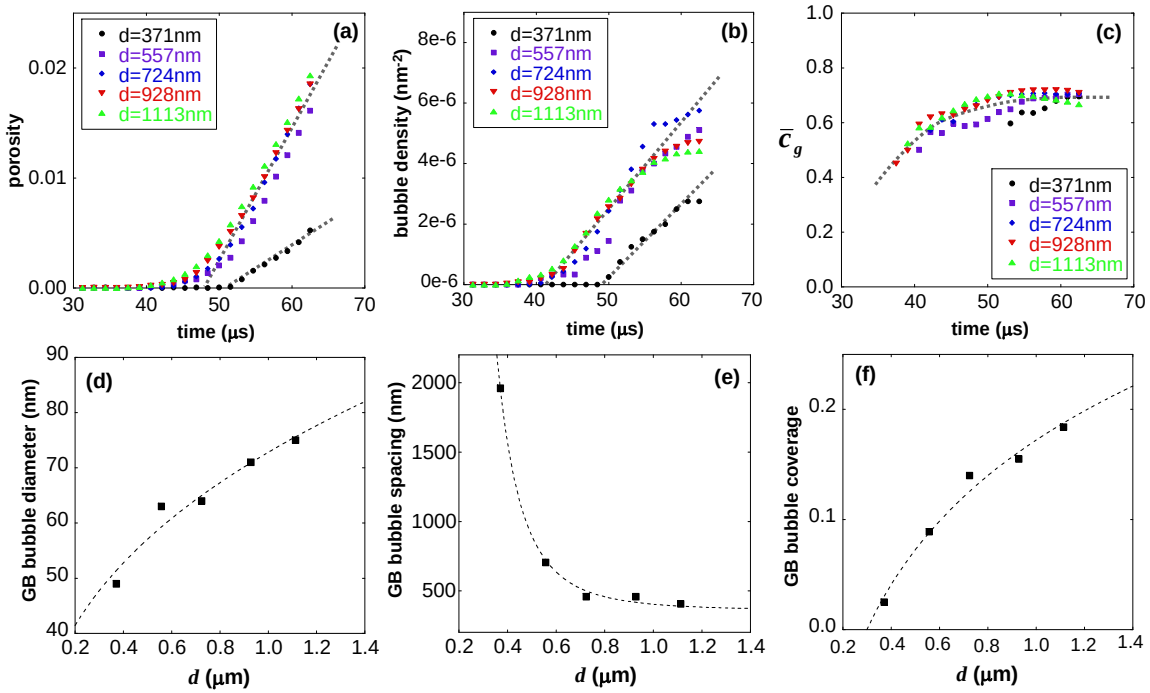

Figure 11: Characteristics of intergranular gas bubbles for different grain sizes. The (a) porosity, (b) bubble density, and (c) gas concentration within the bubbles does not vary substantially for the different grain sizes. However, as the grain size increases, the (d) average bubble diameter increases, the (e) average GB bubble spacing decreases, and the (f) GB bubble coverage increases. (The data for (d), (e), and (f) are taken at the end of the simulations, t = 62 μs).

Binary alloy (concentrated systems)

Dubey, El-Azab

- On-lattice species: V, A, B; 3 types of (dumbbell) interstitials AA, AB, BB

- 6 conserved order parameters (6 coupled diffusion-reaction equations) + microstructure equations

- Complex free energy expression – free energy represents the atomic configuration (obtain by statistical coarse graining)

- Complex kinetics of diffusion and reactions

- **Concurrent microstructure and micro-chemical changes**

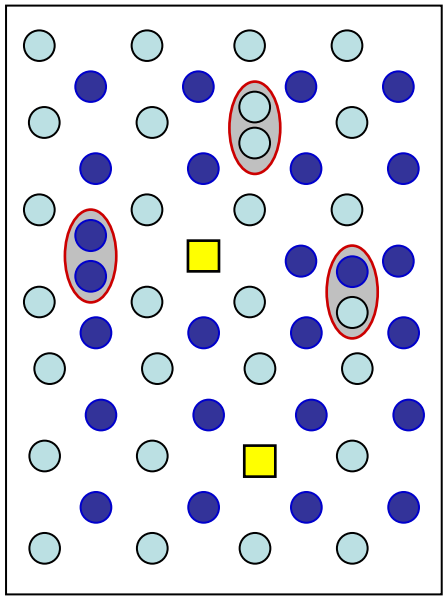

Alloy free energy (no microstructure)

Free Energy of the alloy without defects is given as:

$$\frac{F}{N} = \frac{z}{2}\left[c_A V_{AA} + c_B V_{BB} + c_A c_B \Omega_{AB}\right] + kT\left[c_A log c_A + c_B log_e c_B + 3log\left(\frac{kT}{h\nu_E}\right)\right]$$

N = Total number of lattice sites,
z = Co-ordination number of the crystal,
c_i = concentration of ith species $(i = A, B)$,
$\Omega_{AB} = 2V_{AB} - V_{AA} - V_{BB}$ = interaction parameters,
V_{ij}, $(i,j = A, B)$ = bond enthalpy of ij bond,
ν_E = Einstein's frequency of vibration.

When vacancies are present, the free energy is given as below:

$$\frac{F}{N} = c_v E_v^f + \frac{z}{2}\left[c_A V_{AA} + c_B V_{BB} + c_v V_{vv} + \Omega_{AB} c_A c_B + \Omega_{AV} c_A c_v + \Omega_{BV} c_B c_v\right]$$
$$+kT\left[c_A log_e c_A + c_B log_e c_B + c_v log_e c_v + 3log\left(\frac{kT}{h\nu_E}\right) + \alpha c_v log\left(\frac{\nu_E}{\nu_v}\right)\right]$$

Where, E_v^f = enthalpy of formation of a vacancy,
αc_v = number of vibarional modes affected due to presence of vacancies,
ν_v = Vibrational frequency of the affected modes due to vacancy,
ν_E = Vibrational frequency of the unaffected modes.
In compact form, we can write the above equation as:

$$\boxed{\frac{F}{N} = c_v E_v^f + \frac{z}{2}\left[\sum_{i=1}^{n_s} c_i V_{ii} + \frac{1}{2}\sum_{i=1}^{n_s}\sum_{j=1}^{n_s} c_i c_j \Omega_{ij}\right] + kT\left[\sum_{i=1}^{n_s} c_i log_e c_i + 3log\left(\frac{kT}{h\nu_E}\right) + \alpha c_v log\left(\frac{\nu_E}{\nu_v}\right)\right]}$$

n_s = Number of species present in the system (A, B, V).

With interstitials:

$$\frac{F}{N} = \sum_{i=1}^{n_d} c_i E_i^f + \frac{z}{2}\Big[\sum_{k=1}^{n_s} c_i V_{ii} + \frac{1}{2}\sum_{i=1}^{n_s}\sum_{j=1}^{n_s} c_i c_j \Omega_{ij}\Big] + kT\Big[\sum_{i=1}^{n_s} c_i \log_e c_i + 3\log\Big(\frac{kT}{h\nu_E}\Big) + \sum_{j=1}^{n_d} \alpha_j c_j \log\Big(\frac{\nu_E}{\nu_j}\Big)\Big]$$

where, $\Omega_{ij} = 2V_{ij} - V_{ii} + V_{ij}$,

n_d = Type of defects in the system $(V, I_{AA}, I_{BB}, I_{AB})$,

n_s = Number of species in the system $(A, B, V, I_{AA}, I_{BB}, I_{AB})$,

$\alpha_j c_j$ = Number of vibrational modes affected because of jth defect ,

ν_j = Vibrational frequency of the affected mode due to j^{th} defect.

Oxide materials (MO_2)

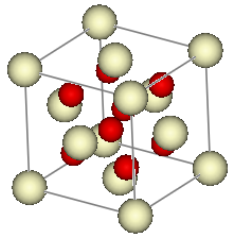

- Vacancies and interstitials on 2 sublattices
- Anti-site defects
- Substitutional gas or metal atoms

} Point defects

- Dislocation loops, voids, grain boundaries, precipitates, etc.

} Microstructure

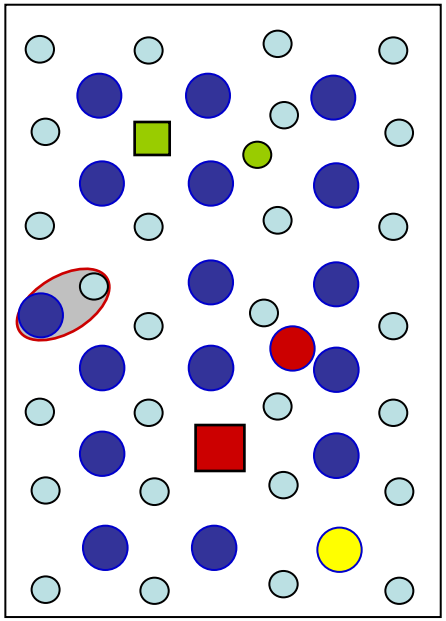

- Complex free energy expression; complex kinetics of diffusion and reactions
- Electrostatic and stress fields

Preliminary model for MO_2

Free energy functional

$$F = \int_v \Big[h(\eta)\left(N_o f_o^s(c_v^o, c_i^o) + N_u f_u^s(c_v^u, c_i^u)\right) + j(\eta)\left(N_o f_o^v(c_v^o, c_i^o) + N_u f_u^v(c_v^u, c_i^u)\right)$$
$$+ \frac{N_o \kappa_v^o}{2}|\nabla c_v^o|^2 + \frac{N_o \kappa_i^o}{2}|\nabla c_i^o|^2 + \frac{N_u \kappa_v^u}{2}|\nabla c_v^u|^2 + \frac{N_u \kappa_i^u}{2}|\nabla c_i^u|^2 + \frac{(N_u + N_o)\kappa_\eta}{2}|\nabla \eta|^2 + E_e \Big] dV$$

Defect energy

$$f_o^s = c_v^o E_v^o + c_i^o E_i^o + k_b T\left[c_v^o \ln(c_v^o) + c_i^o \ln(c_i^o) + (1 - c_v^o - c_i^o)\ln(1 - c_v^o - c_i^o)\right] \qquad f_o^v = (c_v^o - 1)^2 + c_i^{o2}$$

$$f_u^s = c_v^u E_v^u + c_i^u E_i^u + k_b T\left[c_v^u \ln(c_v^u) + c_i^u \ln(c_i^u) + (1 - c_v^u - c_i^u)\ln(1 - c_v^u - c_i^u)\right] \qquad f_u^v = (c_v^u - 1)^2 + c_i^{u2}$$

Kinetic equations

$$\boxed{\begin{aligned}
\frac{\partial c_v^o}{\partial t} &= \nabla \cdot \left(M_v^o \nabla \frac{1}{N_o}\frac{\partial F}{\partial c_v^o}\right) + P_v^o - R_{iv}^o(c_v^o, c_i^o, \eta) \\
\frac{\partial c_i^o}{\partial t} &= \nabla \cdot \left(M_i^o \nabla \frac{1}{N_o}\frac{\partial F}{\partial c_i^o}\right) + P_i^o - R_{iv}^o(c_v^o, c_i^o, \eta) \\
\frac{\partial c_v^u}{\partial t} &= \nabla \cdot \left(M_v^u \nabla \frac{1}{N_u}\frac{\partial F}{\partial c_v^u}\right) + P_v^u - R_{iv}^u(c_v^u, c_i^u, \eta) \\
\frac{\partial c_i^u}{\partial t} &= \nabla \cdot \left(M_i^u \nabla \frac{1}{N_u}\frac{\partial F}{\partial c_i^u}\right) + P_i^u - R_{iv}^u(c_v^u, c_i^u, \eta)
\end{aligned}}$$

$$\boxed{\frac{\partial \eta}{\partial t} = -L \frac{1}{N_u + N_o}\frac{\partial F}{\partial \eta} + P_\eta}$$

Subsidiary electrostatic problems

$$E_e = \frac{1}{2}\int_V \phi(\mathbf{r})\,\rho(\mathbf{r})\,dV \qquad \rho(\mathbf{r}) = q_v^o c_v^o(\mathbf{r}) N_o + q_i^o c_i^o(\mathbf{r}) N_o + q_v^u c_v^u(\mathbf{r}) N_u + q_i^u c_i^u(\mathbf{r}) N_u \qquad -\frac{\rho(\mathbf{r})}{\epsilon_0} - \nabla^2 \phi(\mathbf{r}) = 0$$

Subsidiary elastic problems

Eigen strain problem

Summary

Phase field models have been developed for a range or irradiation problems.

Initial results show that the approach is very promising.